thermo

Article

Packed Bed Thermal Energy Storage System: Parametric Study

Ayah Marwan Rabi', Jovana Radulovic and James M. Buick *

School of Mechanical and Design Engineering, University of Portsmouth, Portsmouth PO1 3DJ, UK; ayah.rabi3@myport.ac.uk (A.M.R.); jovana.radulovic@port.ac.uk (J.R.)
* Correspondence: james.buick@port.ac.uk

Abstract: The use of thermal energy storage (TES) contributes to the ongoing process of integrating various types of energy resources in order to achieve cleaner, more flexible, and more sustainable energy use. Numerical modelling of hot storage packed bed storage systems has been conducted in this paper in order to investigate the optimum design of the hot storage system. In this paper, the effect of varying design parameters, including the diameter of the packed bed, the storage material, the void fraction, and the aspect ratio of the packed bed, on storage performance was investigated. COMSOL Multiphysics 5.6 software has been used to design, simulate, and validate an axisymmetric model, which was then applied to evaluate the performance of the storage system based on the total energy stored, the heat transfer efficiency, and the capacity factor. In this paper, a novel-packed bed was proposed based on the parametric analysis. This involved a 0.2 void fraction, 4 mm porous media particle diameter, and Magnesia as the optimum storage material with air as the heat transfer fluid.

Keywords: packed bed; PTES; parametric study; particle diameter; aspect ratio; porosity; porous media; COMSOL; optimisation

check for updates

Citation: Rabi', A.M.; Radulovic, J.; Buick, J.M. Packed Bed Thermal Energy Storage System: Parametric Study. *Thermo* **2024**, *4*, 295–314. https://doi.org/10.3390/thermo4030016

Academic Editor: Luisa F. Cabeza

Received: 16 May 2024
Revised: 5 July 2024
Accepted: 8 July 2024
Published: 10 July 2024
Corrected: 17 January 2025

1. Introduction

Storage of energy is crucial to overcome the mismatch between variations in energy demand and renewable generation. Renewable sources of energy are intermittent, as they can be affected by weather conditions or other factors. Therefore, storing excess energy during times of low demand and using it later when the energy demand is higher is important to mitigate the high demand for these intermittent resources. One effective solution to overcome this challenge is to use energy storage systems [1].

Pumped Thermal Energy Storage (PTES) is a promising technology for large-scale energy storage. Compared to other thermal energy storage methods, PTES offers high round-trip efficiency (RTE), high capacity, a lifespan of up to 30 years, a short response time [2–4], and a fast start-up time [5,6]. PTES systems are not only environmentally friendly but also have a smaller carbon footprint compared with other novel large-scale commercialised energy storage technologies, such as Compressed Air Energy Storage (CAES) and Pumped Hydro Energy Storage Systems (PHES) [7,8].

During the charging process of PTES systems, electrical energy is converted into thermal energy. This is performed using a heat pump that moves heat from a low-temperature reservoir to a high-temperature reservoir. Later, during the discharging process, the thermal energy stored in the reservoirs is used to power a heat engine. The heat engine then converts the thermal energy back into electrical energy. The conventional layout of PTES is shown in Figure 1 [1].

There are various TES systems; nonetheless, the packed bed is one of the preferred designs with some limitations based on the type of application [9–12]. The packed bed storage system (PBSS) is a compact structure that offers a high heat storage capacity, a large surface area, an efficient energy transfer process, and very efficient storage.

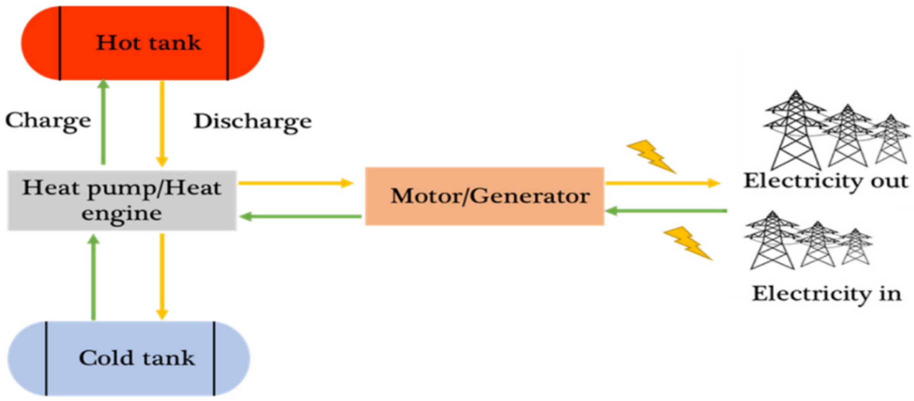

Figure 1. PTES conventional layout and main components [1].

The PBSS is an encouraging TES technology that helps enhance renewable energy generation systems and reduce energy storage costs [13,14]. The PBSS is an efficient technology that can be used for a wide range of temperatures, making it suitable for both high- and low-temperature applications [14,15].

The PBSS system consists of three main components: the mechanism of thermal energy transfer, the storage medium, and the containment system. The bed itself, see Figure 2, is made up of storage materials, such as rocks, PCM, ores, or concrete, depending on factors such as economic considerations, intended use or application, and energy storage capacity [16].

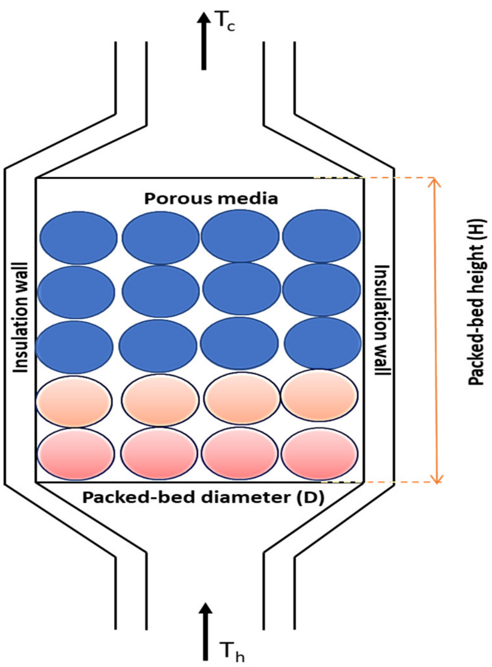

Figure 2. A schematic illustration of a packed bed thermal store with hot HTF entering from the bottom at temperature T_h and exiting from the top at temperature T_c.

During both the charging and discharging phases, it is important to maintain contact between the heat transfer fluid (HTF) and the packing elements that circulate the bed voids to add or remove heat to the solid material. This increases the effective area of surfaces that are in contact, which in turn help to improve efficiency [17]. Additionally, by adding improved stratification to the PBSS, the collector efficiency can be increased [18].

High-temperature thermal energy storage is becoming increasingly important as a key component in large-scale applications. Packed bed storage represents an economically viable large-scale energy storage solution.

A wide range of applications, including chemical and drying processes, reactor designs, and thermal storage, have been studied in the literature concerning heat transfer within packed beds.

The first analysis of packed bed temperature transients dates back to 1926 and was undertaken by Anzelius [19]. This later developed into the well-known Schumann model in 1929 [20], which is essentially a one-dimensional, 'two-phase' model allowing for temperature differences between the gas and solid.

Various numerical schemes based on the Schumann approach have since been developed and validated by measurements [21]. Schumann's model [20,22,23], which models fluid flow through a packed bed of solid spheres as a flow through porous media, is a frequently used basic two-phase model. Sanderson et al. [24] and Regin et al. [25] use this model to study the effect of various parameters, such as particle diameter on axial dispersion and pressure drop. The size of particles has a significant impact on the heat transfer area, which in turn affects the temperature of the fluid as it moves through the packed bed. The main factor that is affected by particle diameter is the permeability, which equals [26] the following:

$$k = \frac{d_p^2 \varepsilon^3}{150 * (1 - \varepsilon^2)} \tag{1}$$

according to the Ergun model for non-Darcy flow, k is the permeability, d_p is the particle diameter, and ε is the porosity.

Based on the equation, if the particle diameter increases, the permeability will increase while the porosity remains constant—permeability is the property of porous materials that describes the ease with which a substance, such as a fluid or gas, can flow through the interconnected void spaces within the material. The explanation for this relation is that larger particles create more open structures between them, which creates greater void spaces. This facilitates easier fluid movement through the porous medium. Essentially, permeability is a measure of how easily fluids can move through a porous material.

The relationship between particle size and efficiency can be understood as follows: heat transfer within the packed bed depends heavily on the surface area of the particles. Smaller particles have a greater surface area compared to larger ones, which leads to increased interaction between the fluid and the porous material. As a result, heat is transferred more effectively from the fluid to the solid, resulting in a higher heat transfer. Therefore, smaller particles tend to have higher thermal efficiency in applications related to heat storage.

Recently, Navier–Stokes-based 3D optimisation studies were performed by Bataineh et al. [27]. From the above literature, it is observed that there is no particular theory for the precise size selection of TES systems.

Singh et al. [16] provided a brief review of analytical models and experimental work. However, experiments can be expensive and require a numerical simulation approach to predict the complex transient of storage systems. Recent reviews of analytical or numerical models are given by Gracia et al. [28] and Elouali et al. [29].

The storage of thermal energy can be divided into three categories, with each method designed for different purposes. Sensible Heat Storage (SHS) is a widely used technique for storing and releasing thermal energy by altering the temperature of a medium. Latent Heat Storage (LHS) involves the energy gained or lost during the transformation of a substance from solid to liquid, or vice versa. This method is commonly used in low-temperature applications, and the materials used in this category are known as Phase Change Materials (PCMs) Lastly, Thermochemical Energy Storage is a method that uses reversible chemical reactions to store and release thermal energy. This method has a high energy density and can be used in various applications.

Several packed bed designs are available in the literature, varying in geometry, storage medium, and heat transfer fluid (HTF). Typically, the HTF travels axially through the store, which is cylindrical. The filler is usually a solid substance such as ceramics, alumina, or crushed rock. Packed beds of this type are classified as SHS because the thermal change in the filler is responsible for storing energy. As an alternative, PCMs that are encapsulated can also be used to create LHS systems [30], but this can increase the cost and complexity of the system.

HTFs can exist in the form of gases, such as air [18,31] or argon [28], or liquids, such as thermal oils [29] or molten salts [25]. A packed bed storage facility operates in two different ways, depending on whether it is being charged or discharged. When heat is added to the bed, the flow usually moves in one direction, and when heat is removed, the flow moves in the opposite direction.

This paper applies numerical modelling using COMSOL Multiphysics software to investigate the performance of a thermal energy storage-packed bed system. A parametric study is conducted to determine the optimum design parameter values, such as the particle diameter of the porous media, void fraction, storage material, and aspect ratio, in order to enhance the hot storage packed bed's overall performance.

2. Methodology

A 2D axisymmetric cylindrical model is constructed using COMSOL Multiphysics 5.3. The hot tank consists of a fully insulated reservoir with a vertical configuration. As an initial step, the model was set up based on Meier et al. [32], and then the model was upscaled and validated for high-temperature thermal storage against the results of White et al. [33]. The results from COMSOL Multiphysics were based on the numerical solution of the heat transfer and fluid flow in porous media. The developed model was optimised across a range of design parameters.

2.1. Governing Equations

The model used to simulate packed beds in this paper is a modified version of the widely used one-dimensional Schumann equations [20]. The approach is based on an extension of the Schumann model, and it relies on the following assumptions:

- The heat transfer between the gas and solid is limited by the thermal resistance at the particle surface. This assumption is based on the small size of the particles and the resulting low Biot numbers.
- The axial direction longitudinal conduction through the bed and heat leakage to the surroundings occurs through and from the solid. This is performed for convenience.
- The kinetic and potential energy terms for the gas flow are negligible.
- The heat transfer problem was solved numerically by using COMSOL Multiphysics software. The solution was based on the local thermal nonequilibrium equation, Fourier's law, and non-Darcian flow. To describe the transfer of heat in a porous medium, the local thermal nonequilibrium hypothesis uses two temperature fields.
- The applied conventional momentum and continuity equations are shown in Equations (2) and (3) [34] as follows:

$$\frac{\partial\left(\rho\vec{u}\right)}{\partial(\varepsilon t)}+\frac{\nabla.\left[\rho\vec{u}\vec{u}\right]}{\varepsilon^{2}}=\nabla.\left(\mu\nabla\vec{u}\right)-\nabla p+\rho\vec{g}-\left(\frac{\mu}{k}+\frac{C_{F}\rho}{\sqrt{k}}\left|\vec{u}\right|\right)\left|\vec{u}\right| \quad (2)$$

$$\frac{\partial(\varepsilon\rho)}{\partial t}+\nabla.\left[\rho\vec{u}\right]=0 \quad (3)$$

where ρ is the porous media density, μ is the porous media viscosity, C_F is the Forcheimer parameter, and $\vec{u}=u_r\vec{e}_r+u_x\vec{e}_x$ represents the superficial velocity vector based on the total cross-sectional area of the porous media and the HTF.

- Additionally, the Shuman method solves two coupled energy equations independently: one for solids and one for the HTF. Equations (4) and (5) can be used to explain this theory [26].

$$\theta_s \rho_s c_{p.s} \frac{\partial T_s}{\partial t} + \nabla.q_s = q_{sf}\left(T_f - T_s\right) + \theta_s Q_s \tag{4}$$

$$\varepsilon \rho_f c_{p.f} \frac{\partial T_f}{\partial t} + \rho_f c_{p.f} u_p.\nabla T_f + \nabla.q_f = q_{sf}\left(T_s - T_f\right) + \varepsilon Q_f \tag{5}$$

where θ_s is the solid volume fraction; ε is the material porosity (void fraction); ρ_s is the solid density; ρ_f is the fluid density; $c_{p.s}$ is the solid heat capacity at constant pressure; $c_{p.f}$ is the fluid heat capacities at constant pressure; q_s is the solid conductive heat flux; q_f is the fluid conductive heat flux; q_{sf} is the coefficient of the interstitial convective heat transfer; Q_s is the solid heat source; Q_f is the fluid heat source; Q_{ted} is the thermoelastic damping contribution straight from the solid mechanics interfaces; q is the conductive heat flux; ∇ is the gradient operator; Q_{vd} is the viscous dissipation in the fluid; u_p is the porous velocity vector; T_s is the temperature of the solid; T_f is the temperature of the fluid; τ is the viscous stress tensor; S is the second Piola–Kirchhoff tensor; and $\frac{\partial S}{\partial t}$ is the operator and the material derivative.

COMSOL utilises Equations (6) and (8) to numerically solve the heat transfer in solid storage material [26].

$$\rho_f c_p u.\nabla T_s + \nabla.q = Q_s + Q_{ted} \tag{6}$$

$$Q_{ted} = -\alpha T : \frac{\partial S}{\partial t} \tag{7}$$

$$q_s = -K_s \nabla T \tag{8}$$

Equations (9) and (11) solve the heat transfer in heat transfer fluid numerically [26] as follows:

$$\rho_f c_p u_p.\nabla T_f + \nabla.q_f = Q_f + Q_p + Q_{vd} \tag{9}$$

$$Q_{vd} = \tau : \nabla u \tag{10}$$

$$q_f = -K_f \nabla T_f \tag{11}$$

In the context of the local thermal nonequilibrium hypothesis, a recall to the modified version of Fourier's law of conduction is shown in Equations (12) and (13) [26].

$$q_s = -\theta_s K_s \nabla T_s \tag{12}$$

$$q_f = -\varepsilon K_f \nabla T_f \tag{13}$$

where K_s and K_f are the thermal conductivity for the solid and fluid respectively and ε is the porosity.

The Local Thermal Nonequilibrium Interface is a predefined connection between the heat transfer that occurs within solids and the heat transfer that occurs within fluids.

Darcy's law is the fundamental principle governing fluid flow in porous materials, describing a direct relationship between velocity and pressure gradient. This law is only valid at very low velocities or low Reynolds numbers (Re < 10). In cases of relatively fast flow (10 < Re < 1000), Darcy's linear relation between velocity and pressure drop no longer applies, and the non-Darcian/Ergun model becomes more suitable. A general expression for the nonlinear relationship between the pressure gradient and velocity can be written as follows [26]:

$$-\nabla p = \frac{\mu}{k}\vec{u} + \frac{C_F}{\sqrt{k}}\rho \vec{u}\left|\vec{u}\right| \tag{14}$$

where C_F is the Forcheimer parameter, and it is dimensionless, k is the permeability, and u is the fluid velocity vector.

The flow regime through a packed bed can be classified based on the Reynolds number of the bed, which is calculated using the particle size. A Reynolds number between 150 and 300 suggests a hydrodynamic dispersive flow due to spatial deviation [35]. Table 1 presents the flow regimes defined in various literature sources [36].

Table 1. The fluid flow regime based on the Reynolds number.

The Fluid Flow Regime	The Reynolds Number Range
Darcy or creeping flow regime	Re < 10
Forchheimer flow regime	10 < Re < 150
Post-Forchheimer flow regime	150 < Re < 300
Fully turbulent flow regime	Re > 300

This paper uses the standard Reynolds-averaged Navier–Stokes (RANS) standard k-ε model to solve the fluid flow in the porous media using Equations (15) and (16) [26] as follows:

$$\rho(u.\nabla)k = \nabla.\left(\left(\mu + \frac{\mu_T}{\sigma_k}\right)\nabla k\right) + P_k - \rho\varepsilon \tag{15}$$

$$\rho(u.\nabla)\varepsilon = \nabla.\left(\left(\mu + \frac{\mu_T}{\sigma_\varepsilon}\right)\nabla \varepsilon\right) + C_{\varepsilon 1}\frac{\varepsilon}{k}P_k - C_{\varepsilon 2}\rho\frac{\varepsilon^2}{k} \tag{16}$$

where $\mu_T = \rho C_\mu \frac{k^2}{\varepsilon}$, C_μ is the k-ε based model constant, $P_k = \mu_T\left(\nabla u : \left(\nabla u + (\nabla u)^T\right) - \frac{2}{3}(\nabla.u)^2\right)$ $-\frac{2}{3}\rho k \nabla.u$, μ is the dynamic viscosity of the fluid, μ_T is the eddy viscosity, and $C_{\varepsilon 1}$, $C_{\varepsilon 2}$, σ_ε, σ_k are the constants [36].

The Reynolds number has been calculated using Equation (17) [26] as follows:

$$Re = \frac{d_p \rho |u|}{(1-\varepsilon)\mu} \tag{17}$$

In the current paper, the flow regime is fully turbulent, where the Reynolds number is $Re > 300$.

2.2. Initial Model Set Up and Validation

To verify the accuracy of the numerical analysis performed in COMSOL Multiphysics, an initial model small was built up, tested, and validated based on Meier's study [32]. The initial model dimensions and operating parameters are shown in Table 2.

Table 2. Meier's model operating parameters and the main setup [32].

Storage Tank	Symbol	Unit	Value
Packed Bed Tank			
Tank Diameter	D	m	0.70
Tank Hight	H	m	1.93
Charging Temperature	T_{ch}	°C	27.00
Discharging Temperature	T_{dis}	°C	600.00
Operating Conditions			
Particle Diameter	d_p	mm	2.00
Mass Flow Rate	$\dot{m}$	Kg/s	1.10
Porosity	ε	-	0.45
HTF/Air			
Density	ρ	kg/m^3	1.23
Thermal Conductivity	K	W/(m·K)	11.00
Specific Heat Capacity	c_p	J/(kg·K)	1009.00

After validating the initial model, the model was upscaled based on White's study [33] in order to build a commercialised tank size. The dimensions and operating parameters are presented in Table 3.

Table 3. Geometry and operating parameters of the hot PTES tanks.

Storage Tank	Symbol	Unit	Value
	PTES (Hot Tank)		
Tank Diameter	D	m	4.62
Tank Hight	H	m	4.62
Charging Temperature	T_{ch}	°C	476.00
Discharging Temperature	T_{dis}	°C	25.00
	Operating Conditions		
Particle Diameter	d_p	mm	4.00
Operating Pressure	P	Bar	10.50
Mass Flow Rate	$\dot{m}$	Kg/s	13.70
Porosity	ε	-	0.40

The model boundary conditions have been set up as a zero-velocity no-slip wall. At the inlet, the boundary condition is fully developed with constant mass flow rate velocity, while there is a pressure that suppresses backflow at the outlet. Adiabatic boundary conditions are applied at the outer boundary of the insulation material. An incompressible flow was selected for the fluid, and an operating pressure of 10.5 bar was set for the overall system.

For the upscaled model's main set up with Fe_3O_4, the Glass Wool as a wall insulation material and the thermophysical properties for each are presented in Figure 3 and Table 4, respectively.

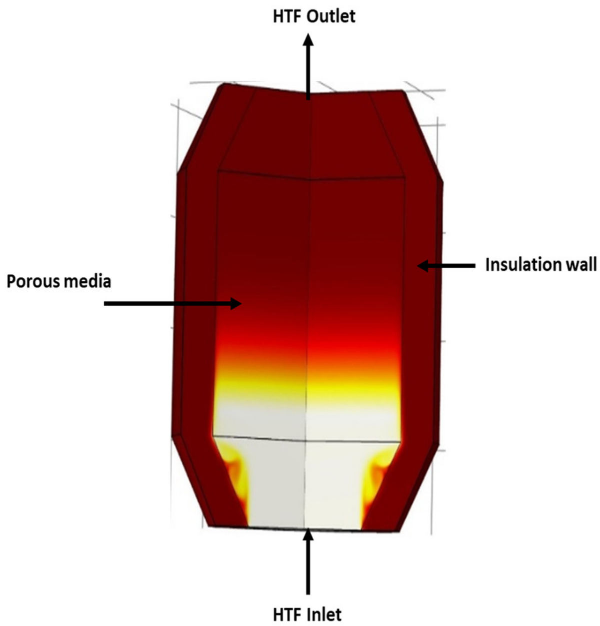

Figure 3. Hot storage tank's main setup.

Table 4. Magnetite (Fe_3O_4) and Glass Wool thermophysical properties [32,33].

Storage Material (Fe_3O_4)	Symbol	Unit	Value
Thermal Conductivity	K	W/(m·K)	3.500
Density	ρ	Kg/m^3	5175.000
		Variable	
Specific Heat Capacity	$c_{p,s}$	J/kg·K	$[104.21 + 178.51 \times T/1000) + 10.62 \times (T/1000)^2 + 1.13 \times (T/1000)^3 - 0.99/(T/1000)^2]/0.23$

Table 4. *Cont.*

Storage Material (Fe_3O_4)	Symbol	Unit	Value
		Insulation Material (Glass Wool)	
Thermal Conductivity	K	W/(m·K)	0.025
Density	ρ	Kg/m^3	1250.000
Specific Heat Capacity	$c_{p,s}$	J/kg·K	850.000

The initial model validation results against Meier et al.'s [32] study are shown in Figure 4.

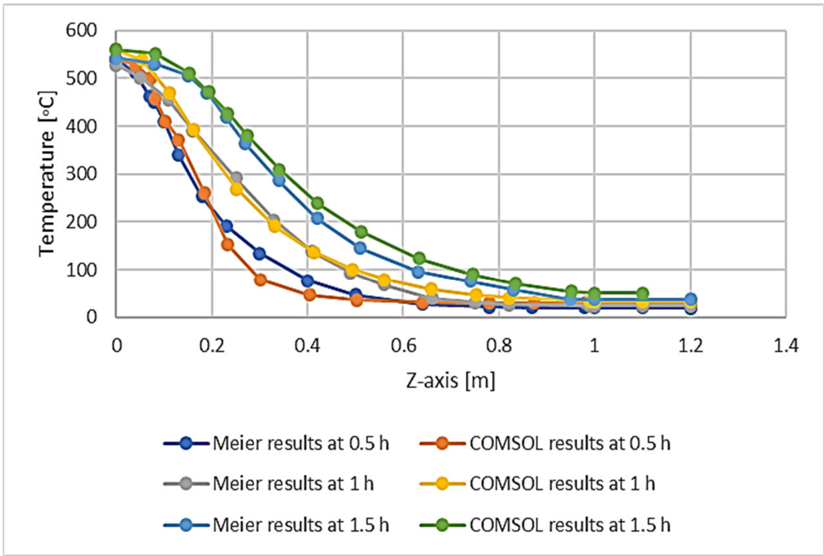

Figure 4. Model validation by comparing Meier's results vs. the numerical results using COMSOL Multiphysics.

The comparison shows good agreement between Meier's study results and the numerical results with only small deviations. The reference work is based on experimental work, while the COMSOL model is based on the numerical method. The agreement between the results is satisfactory and, therefore, considered to validate the numerical model.

2.3. Mesh Validation

COMSOL Multiphysics is used to numerically solve the energy equation inside the solid sensible porous media. The finite element method is used in COMSOL for solving the partial differential equations. Meshing the geometry of the model is performed by predefined triangular mesh sizes. The model is solved for eight different mesh types using the mesh-independent test to find an accurate mesh type. The simulation of the tested mesh resolution has been conducted and compared using the geometry of White et al. [33] after 8 h of charging, as shown in Figure 5.

Figure 5 illustrates the temperature difference between the eight different mesh sizes at three different storage heights (0.5 m, 1.5 m, and 3.5 m) after 8 h of charging compared to the results obtained from the extremely fine mesh (the finest mesh available). The results show a convergence for the finest 4 meshes, indicating their suitability for use in this study. Given that the time requirements for running the simulations were not excessive, the extra fine mesh was selected and is shown in Figure 6.

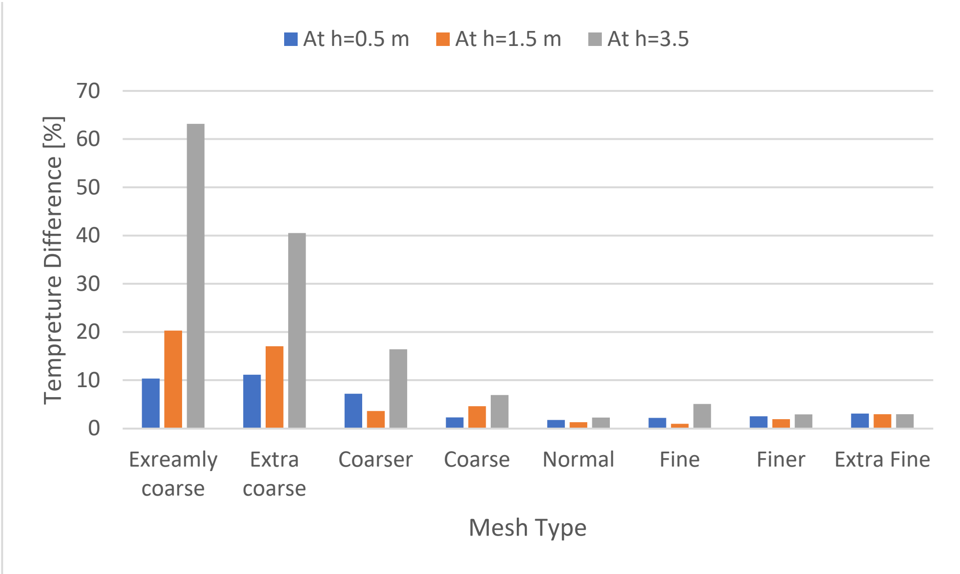

Figure 5. The effect of the mesh size on the temperature difference at t = 8 h.

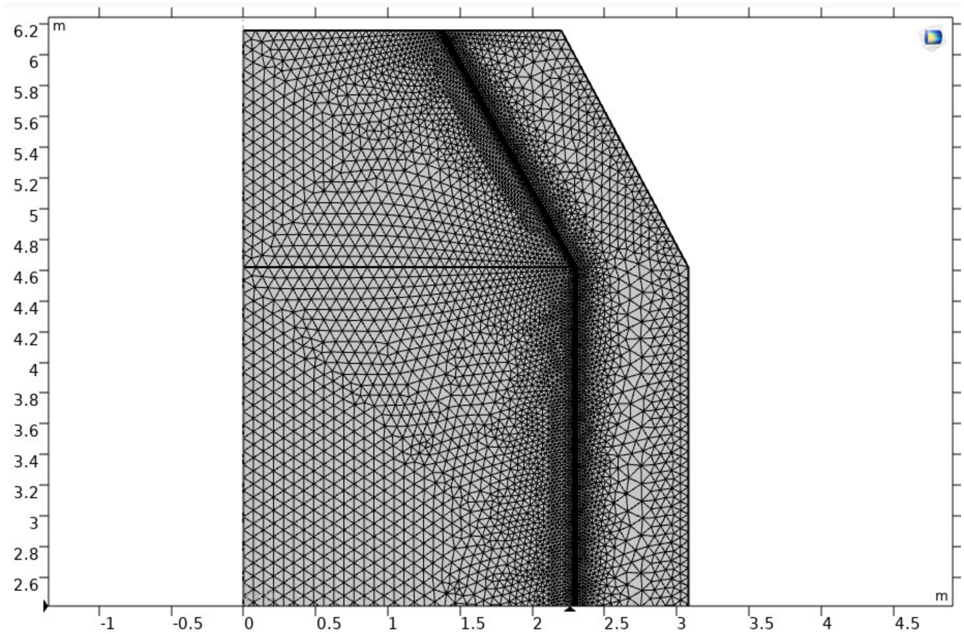

Figure 6. Zoomed-in extra fine mesh generated by COMSOL for initial model validation.

2.4. Model Optimisation

A parametric analysis has been performed in order to optimise the thermal performance of the PTES hot storage design during the charging cycle for large-scale applications. In this regard, four design variables have been investigated: the solid-packed material particle diameter, the solid packing material, the void fraction (material porosity), and the TES tank dimensions (aspect ratio). A summary of the considered variability range for the studied parameters is presented in Table 5.

Table 5. Parametric analysis variables and their range of study.

Medium particle diameter	Full range (4, 20, 40, 80, 100, 120, 140, 160) mm
Solid medium material	NaCL, reinforced concrete, cast iron, silica, and Magnesia.
Void fraction	(0.1, 0.2, 0.4, 0.6)
Aspect ratio (H/D)	(3.65, 2.30, 1.50, 1.00)

Three performance indicators have been used to study the performance of the packed bed with the purpose of finding the optimum design variable values for the storage tank.

- Capacity factor (CF)

This method is based on calculating the useful energy stored after 8 h of the charging cycle divided by the maximum possible thermal energy storage [12], as shown in Equation (18)

$$CF = \frac{\int_0^L (1-\varepsilon)\frac{\pi}{4}D^2\rho_s c_{ps}(T_s - T_{s,i})dz}{(1-\varepsilon)\frac{\pi}{4}D^2\rho_s c_{ps}L\left(T_{fi} - T_{s,i}\right)} \tag{18}$$

Here, the capacity factor (CF) represents the fraction of the total storage capacity that is filled. The governing equation includes several parameters, as well as solid particle and HTF properties. These are shown in Table 3.

- Total energy stored

The second method that has been derived to evaluate the storage tank performance [12] is based on calculating the total energy stored after 8 h of the charging cycle using Equation (19) as follows:

$$\text{E stored} = \int_0^L (1-\varepsilon)\frac{\pi}{4}D^2\rho_s c_{ps}(T_s - T_{s,i})dz \tag{19}$$

- Heat transfer efficiency

According to the assumption from White's study [33], the storage tank design parameters have been evaluated based on the control volume approach for an open system by calculating the stored energy inside the porous media after 8 h of the charging cycle divided by the input energy of the fluid. See Equation (20) [37] as follows:

$$\eta_{HT}(z) = \frac{(T_{s,i} - T_{s,o})}{\left(T_{f,i} - T_{s,i}\right)} \tag{20}$$

Based on the calculation results, the performance of the packed bed hot storage performance has been evaluated in order to find the optimum design variable values.

3. Results and Discussion

This paper presents the development of a hot storage-packed bed model derived from White's model. White's model used argon as an HTF, and Fe_3O_4 was used as the packed storage material, with a particle diameter of 4 mm, a mass flow rate of 13.7 kg/s, and a void fraction of 0.4. The model has a height and width of 4.62 m.

Changing the heat transfer fluid to air is the first step in the model. Next, the particle diameter is examined to determine the optimal value, with a range chosen based on a literature review while maintaining other parameters unchanged. Following the selection of the optimal particle diameter, this paper discusses selecting the optimum porosity and storage material. The optimum particle diameter is then used alongside different packed storage materials and material porosities while maintaining a constant mass flow rate and aspect ratio. The aspect ratio is then tested under constant volume using the optimum particle diameter, material porosity, and storage material. The optimisation results are presented in the sections that follow.

3.1. Optimum Particle Diameters

In this paper, solid particle diameters of 4, 20, 40, 80, 100, 120, and 160 mm were used to investigate the effect of particle size on the performance of the hot storage tank during the charging process. The capacity factor and the total energy stored calculation methods results are shown in Figures 7 and 8, respectively.

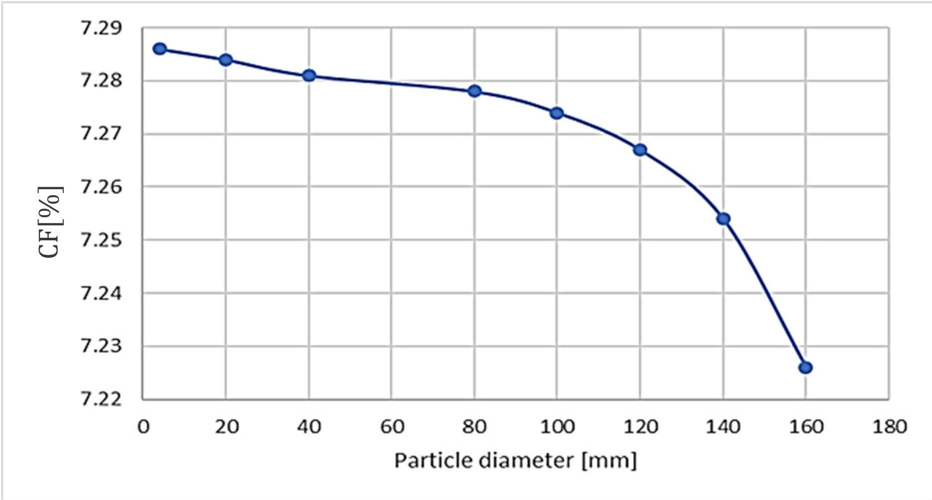

Figure 7. The capacity factor is based on the stored energy versus the particle diameter after 8 h of charging.

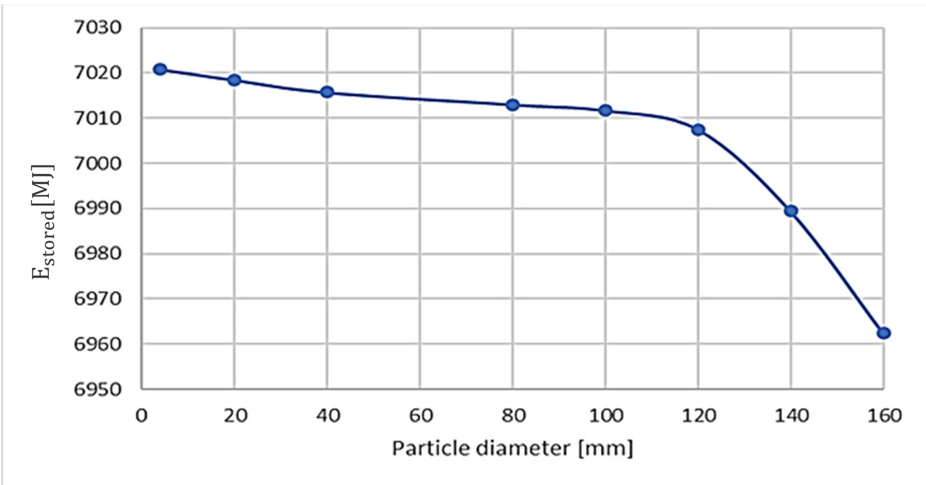

Figure 8. The total stored energy [MJ] versus the particle diameter after 8 h of charging.

According to Figure 7, the capacity factor increases as the particle diameter and the amount of energy stored over the eight hours decrease. Figure 8 shows that the total energy stored increases as the particle diameter size decreases.

The temperature profile of different particle diameters along the packed bed after eight hours of charging is presented in Figure 9.

Based on Figure 9, the temperature of particles with the smallest diameter increases more rapidly than the temperature of particles with the largest diameter. This is due to the fact that the smallest particle diameter has the largest surface area and the greatest number of particles, which enhances the heat transfer performance of the smaller particle sizes.

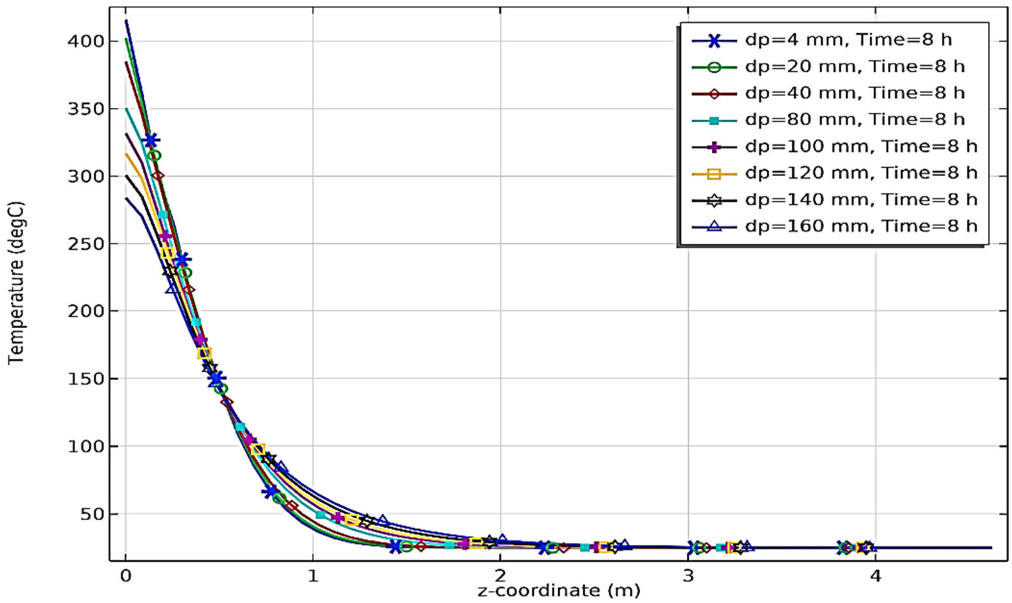

Figure 9. Temperature profile along the *Z*-axis of the packed bed after 8 h of charging time at dp (4, 20, 40, 80, 100, 120, 140, and 160 mm).

Accordingly, Figure 10a illustrates the heat transfer efficiency along the *Z*-axis (packed bed height) after 8 h of charging time; similar results have been provided after 2, 4, and 6 h of charging. It is clear that the heat transfer efficiency profile pattern follows the temperature profile in Figure 9 and agrees with the conclusions obtained in Figures 7 and 8, which show that the smallest particle diameter is associated with the highest performance.

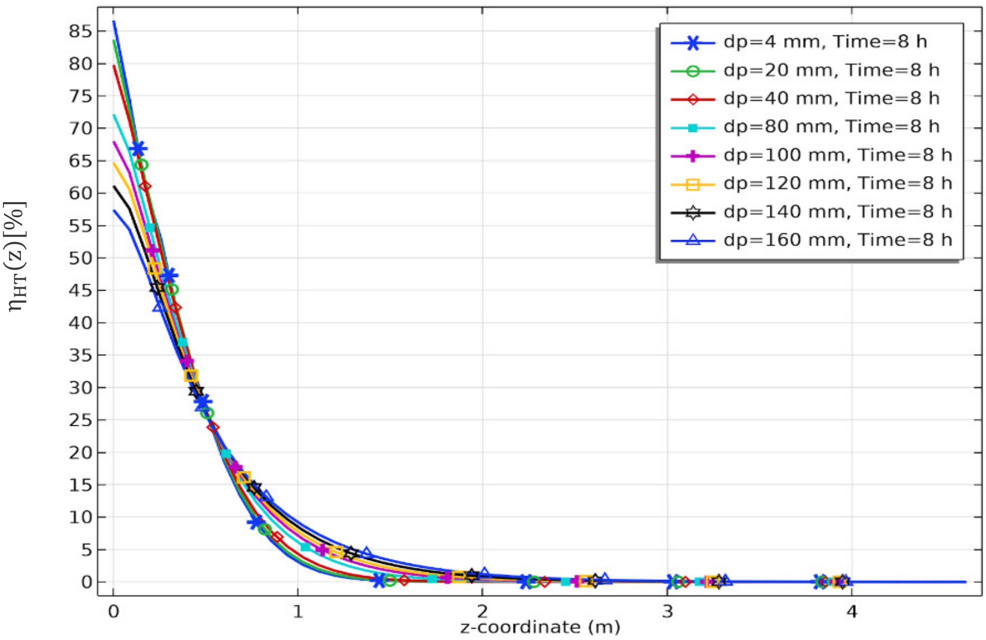

(**a**)

Figure 10. *Cont.*

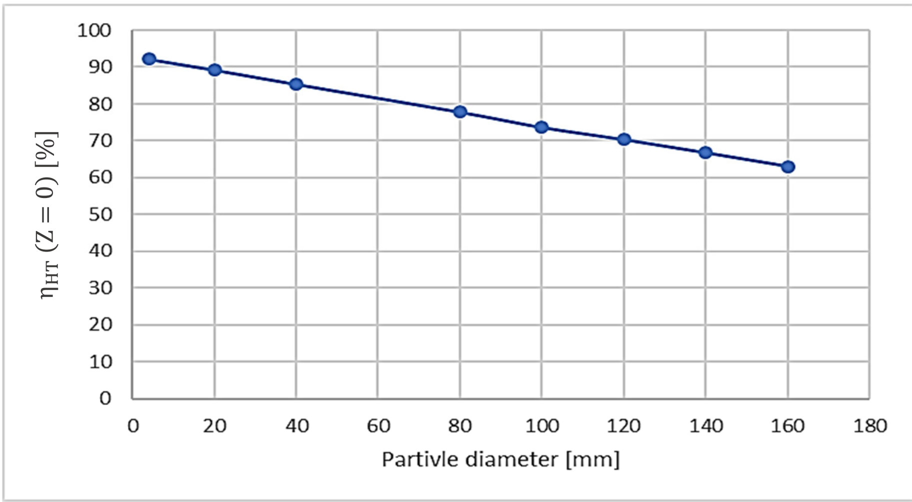

(**b**)

Figure 10. The heat transfer efficiency $\eta_{HT}(z)$ for a range of dp (4, 20, 40, 80, 100, 120, 140, 160 mm) after 8 h of charging. (**a**) The heat transfer efficiency along the *Z*-axis of the packed bed. (**b**) The heat transfer efficiency for each particle diameter size at *Z* = 0.

Figure 10b shows the heat transfer efficiency of each particle size after 8 h of charging. Based on these results, a conclusion is drawn that the smallest particle diameter provides a high energy storage and a more efficient process, which is consistent with the literature review viewpoint.

3.2. Material Selection and Porosity

Storage materials play a crucial role in converting heat energy, as their physical and thermal properties largely determine their effectiveness. To be considered suitable for use, storage materials must possess a high energy density, high heat capacity, high thermal conductivity, long-term cycle stability, good mechanical stability, and low carbon footprint, and also be composed of sustainable, non-toxic materials that are compatible with the intended operating conditions.

In this study, five solid Sensible Heat Storage materials that are suitable for TES systems operating at temperatures above 500 °C have been selected. The thermophysical properties of the selected solid packing materials are shown in Table 6 [6,38,39].

Table 6. Thermophysical properties of different solid packing materials [40,41].

Material	NaCl	Reinforced Concrete	Cast Iron	Silica	Magnesia
c_p [J/Kg·K]	850	850	560	1000	1150
ρ [Kg/m^3]	2160	2200	7200	1820	3000
K [W/m·K]	7.0	1.5	37	1.5	5.0

Porosity refers to the measure of void spaces in a material, and it affects the way fluids flow through it. In fluid dynamics, the impact of porosity on pressure drop is significant, especially in the flow through porous media. The Darcy–Weisbach equation is commonly used to describe pressure drop in porous media. This study selected six different porosity values from 0.1 to 0.6 to find the optimum value for the hot storage design.

Figure 11 presents the relation between the hot tank capacity factor against the material porosity for the different materials considered.

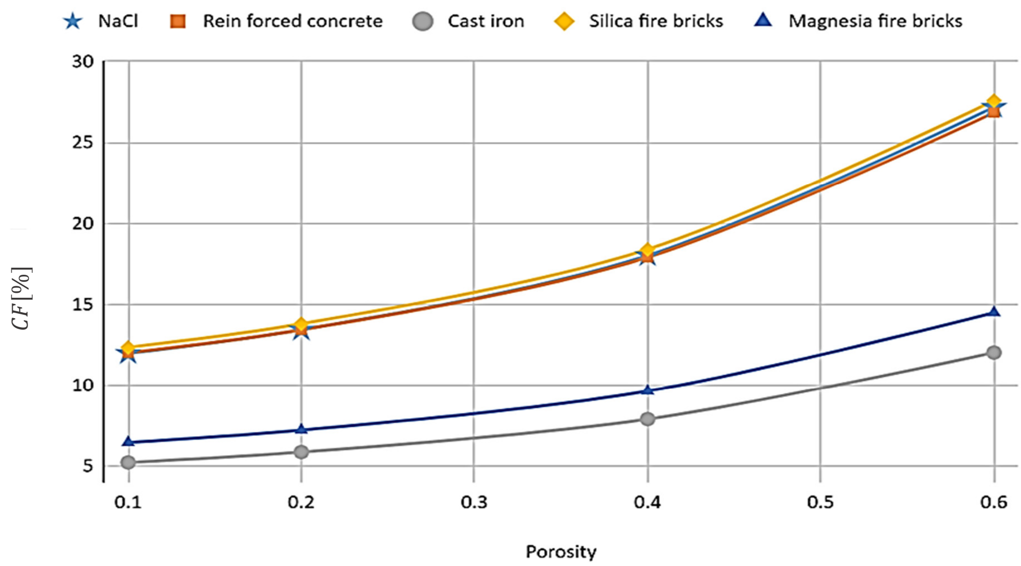

Figure 11. The capacity factor vs. material porosity for 5 solid storage materials.

Figure 11 shows the charging efficiency among five solid sensible storage materials after 8 h of charging. The capacity factor of Magnesia is comparatively low. For instance, at a porosity level of 0.2, the capacity factor of Magnesia is approximately 7%, which signifies it still has the capacity to store up to 14 times as much energy. This also means that if the full capacity is not required, the container could be made smaller. When compared to other materials, like NaCl, reinforced concrete, and silica, Magnesia has a higher charging factor of around 13–14% after 8 h of charging. Although cast iron performs slightly better than Magnesia, it shows poorer performance in Figure 12 with respect to the total energy stored.

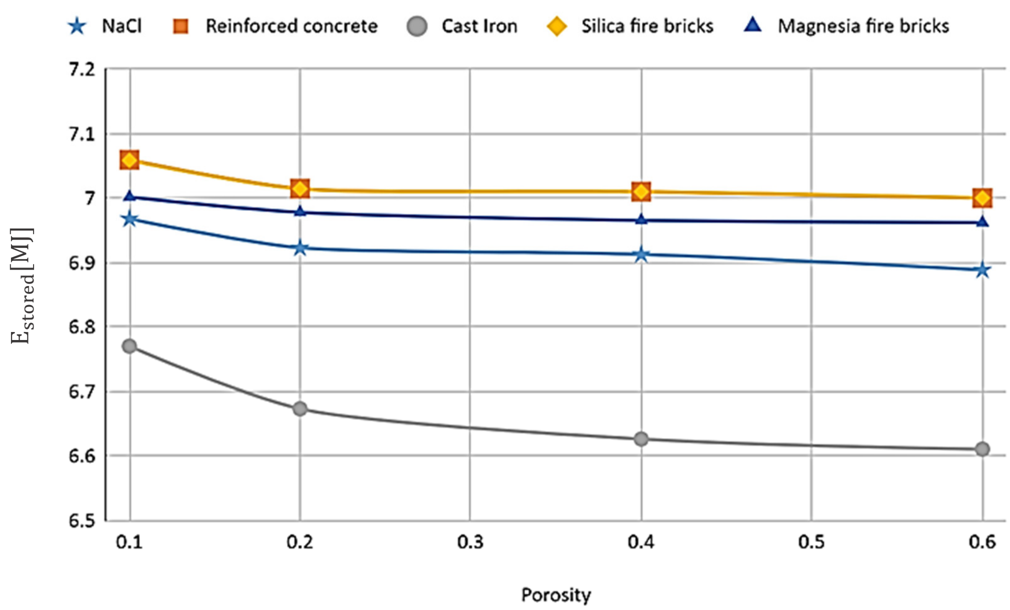

Figure 12. Total energy stored vs. material porosity for 5 solid storage materials.

Figure 12 shows that Magnesia performs well. It stores slightly more than NaCl and slightly lower than reinforced concrete and silica, and they perform much better than cast iron. Although cast iron was seen to perform slightly better than Magnesia in Figure 11, and its poor performance in terms of energy stores, as seen in Figure 12, suggests that it is not an ideal material for the backed bed.

Accordingly, Magnesia performs the second best according to both efficiency and energy stored, and is only slightly behind the silica and reinforced concrete in Figure 12 and the cast iron in Figure 11. In terms of the porosity, it is clear that the total energy stored increases by decreasing the porosity, suggesting that both 0.1 and 0.2 would be appropriate values. However, Figure 13 shows that the pressure drop through the storage container starts to increase at the lower porosity values, so a porosity of 0.2 has been selected.

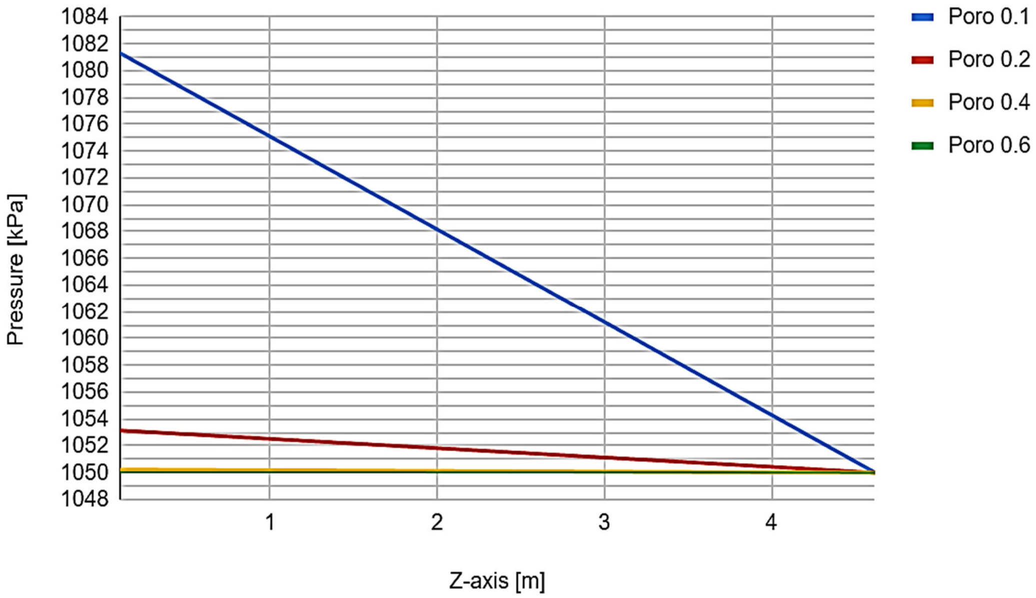

Figure 13. Pressure drop along the porous media height.

After analysing Figures 11–13, it has been concluded that porosity affects the three primary design factors: pressure drop, heat transfer, and energy storage.

3.3. Optimum Aspect Ratio

When designing thermal energy storage tanks for high-temperature applications, it is important to consider the aspect ratio. This ratio affects the efficiency of heat transfer within the storage medium. By optimising the aspect ratio, heat can be distributed effectively throughout the storage material, which is crucial for charging and discharging processes in high-temperature applications.

The aspect ratio in tanks refers to the ratio of the tank's height to its diameter or width. It is a geometric parameter that characterises the shape of the storage tank and is denoted by an aspect ratio = H/D.

Another numerical investigation has been conducted to explore the influence of studying different aspect ratios on the performance of a hot storage tank.

Four different aspect ratios have been tested and conducted in this paper, where the volume of the container was kept fixed, as shown in Table 7.

Table 7. The studied aspect ratio.

Aspect Ratio	h [m]	D [m]	Volume [m^3]
1	4.62	4.62	19.36
1.5	6.00	4.00	19.36
2.3	8.00	3.5	19.36
3.65	10.96	3.00	19.36

The aspect ratio plays a critical role in determining the temperature distribution within the tank. A higher aspect ratio results in a more even temperature distribution, while a lower aspect ratio may cause significant temperature variations from the top to the bottom of the tank. This is because a tank with a higher aspect ratio experiences a smaller temperature gradient along its height, leading to a more homogeneous temperature distribution.

Table 8 shows the effect of changing the aspect ratio on the heat transfer, total energy stored, and system efficiency.

Table 8. Aspect ratio effect on hot storage efficiency.

Capacity Factor [%]				
Time [h]	**Aspect Ratio (1)**	**Aspect Ratio (1.5)**	**Aspect Ratio (2.3)**	**Aspect Ratio (3.65)**
2.00	1.66	1.68	1.76	1.81
4.00	3.30	3.42	3.54	3.62
6.00	4.98	5.22	5.36	5.45
8.00	6.72	7.10	7.21	7.29
Stored Capacity [MJ]				
Time [h]	**Aspect Ratio (1)**	**Aspect Ratio (1.5)**	**Aspect Ratio (2.3)**	**Aspect Ratio (3.65)**
2.00	400.60	405.36	423.78	436.10
4.00	793.64	823.29	853.27	872.21
6.00	1200.35	1257.74	1291.98	1313.48
8.00	1619.02	1701.90	1735.79	1757.25
Heat Transfer Efficiency [%]				
Time [h]	**Aspect Ratio (1)**	**Aspect Ratio (1.5)**	**Aspect Ratio (2.3)**	**Aspect Ratio (3.65)**
2.00	57.66	67.76	77.87	89.28
4.00	75.62	85.06	94.02	99.23
6.00	82.89	91.77	98.86	99.56
8.00	84.69	93.91	99.99	100.00

According to the results shown in Table 8, the highest aspect ratio shows a high-capacity factor, high total energy stored, and high heat transfer efficiency with a slight difference between the amount of energy stored and the system efficiency. The results in Table 8 show that the highest aspect ratio shows a high-capacity factor, high total energy stored, and high heat transfer efficiency. However, the differences are relatively small, and other features should also be considered, such as the increased pressure drop across longer storage devices.

3.4. Temperature Profile

Figure 14 shows the temperature distribution within the storage tank with an aspect ratio of 1 and with the parameters selected based on the optimised parameters found in the preceding analysis. Magnesia is used as the packed bed material with a particle diameter of 4 mm and a porosity of 0.2. This Figure shows the evolution of the temperature distribution within the storage system at selected times over the first four hours of charging and indicates how the temperature profile within the packed bed evolves over the charging process.

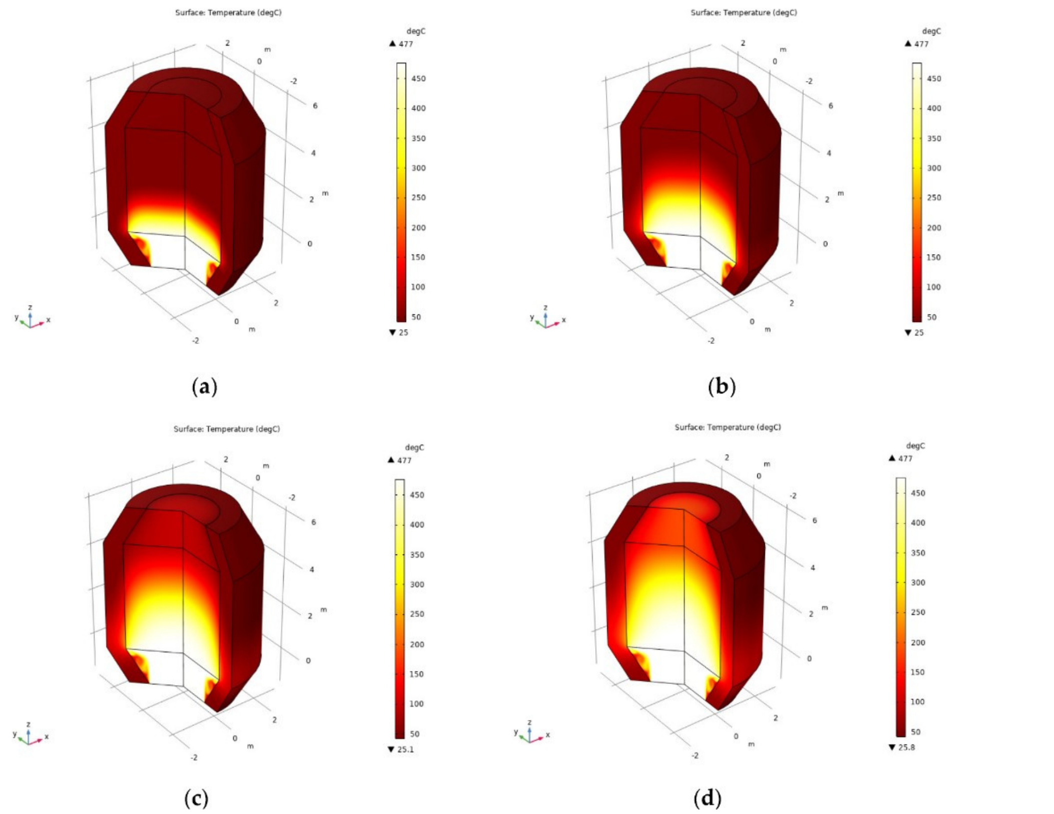

Figure 14. The temperature distribution along the storage tank at different charging times: (**a**) 1 h, (**b**) 2 h, (**c**) 3 h, and (**d**) 4 h.

4. Conclusions

A parametric analysis has been performed in order to optimise the thermal performance of the PTES hot storage design for large-scale applications. Five design parameters have been investigated: the solid-packed material particle diameter; the solid packing material; the material porosity; and the TES tank dimensions (aspect ratio).

In this paper, three performance indicators were applied to evaluate and optimise the performance of the PBSS, including finding the capacity factor, total stored energy, and calculating the methods for calculating heat transfer efficiency during charging the storage tank, which led to the following outcomes:

- The diameter of particles affects the performance temperature profile of a packed bed. Within the range of particle sizes considered here, the smallest diameter of 4 mm demonstrated the optimal performance and was selected because it provided superior performance to the larger particles considered, while at the same time being large enough to make it practical to include in a large-scale commercial system.
- The porosity effects were evaluated against the same performance criteria but also against the pressure drop. The results showed that the capacity and performance of the storage increased with reducing porosity, while the pressure drop increased, which increased the costs and energy consumption while reducing the system efficiency. To achieve a compact design with optimal heat transmission performance and low-pressure drops, a porosity of 0.2 has been selected as an optimum design parameter in this paper.
- Magnesia has been selected based on the results for the total energy stored and the charging capacity. In both cases, Magnesia performed well and was close to being the optimal material. Based on this, Magnesia was selected as having the best overall performance.

- The effect of the aspect ratio on the efficiency of the packed bed was investigated. Based on the results, the highest aspect ratio shows a high-capacity factor, high total energy stored, and high heat transfer efficiency. Conversely, from the pressure drop point of view, as the aspect ratio decreases, the pressure drop increases because the increase in the height of the packed bed increases the losses in the kinetic energy and hence decreases the pressure. Based on that, selecting an aspect ratio with a low-pressure drop that is easy in manufacturing terms has been taken into consideration, and an aspect ratio of 1 has been selected as an optimum parameter in this paper.

In conclusion, this paper found that a PBSS with 0.2 void fractions, an average diameter of the packed bed material of 0.04 m, air as the HTF, Magnesia as the packed bed material, and an aspect ratio of 1 provided a maximum efficiency across the length of the packed bed and have been selected as the optimum parameters for the charging cycle.

Author Contributions: Conceptualisation, J.R. and J.M.B.; methodology, A.M.R., J.R. and J.M.B.; software, A.M.R.; validation, A.M.R.; formal analysis, A.M.R.; investigation, A.M.R., J.R. and J.M.B.; resources, J.R. and J.M.B.; data curation, A.M.R.; writing—original draft preparation, A.M.R.; writing—review and editing, A.M.R., J.R. and J.M.B.; visualisation, A.M.R.; supervision, J.R. and J.M.B.; project administration, J.R. and J.M.B. All authors have read and agreed to the published version of the manuscript.

Funding: This research received no external funding.

Data Availability Statement: Datasets are available upon request from the authors.

Conflicts of Interest: The authors declare no conflicts of interest.

Nomenclature

Abbreviation

TES	Thermal Energy Storage
PBSS	Packed Bed Storage System
PTES	Pumped Thermal Energy Storage
CAES	Compressed Air Energy Storage
PHES	Pumped Heat Energy Storage
RTE	Round Trip Efficiency
HTF	Heat Transfer Fluid
SHS	Sensible Heat Storage
LHS	Latent Heat Storage
PCM	Phase Changed Material

Greek symbols

θ_s	The solid volume fraction
ε	The porosity (void fraction)
α	The thermal diffusivity
σ_ε	Constant = 1.00
σ_ε	Constant = 1.30
∇	The gradient operator

Subscripts

s	Solid
f	Fluid
P	Particle
h	Hot
c	Cold

Roman Symbols

l	The length scale
C	The heat leakage factor
C_f	The coefficient of friction
C_F	The Forcheimer parameter; it is dimensionless
C_μ	k-ε based model constant = 0.09
$C_{\varepsilon 2}$	Constant = 1.92
$C_{\varepsilon 1}$	Constant = 1.44
d_p	The particle diameter
K	Thermal conductivity
k	The permeability
q	The conductive heat flux
qs	The solid material conductive heat fluxes
q_f	The fluid conductive heat fluxes
q_{sf}	The interstitial convective heat transfer coefficient
Q_f	The solid and fluid heat sources
T_h	The inlet's hot temperature
T_c	The outlet's cold temperature
T_s	The porous bed temperature
T_f	The fluid phase temperature
u_p	The porous velocity vector

References

1. Rabi, A.M.; Radulovic, J.; Buick, J.M. Pumped Thermal Energy Storage Technology (PTES): Review. *Thermo* **2023**, *3*, 396–411. [CrossRef]
2. Ge, Y.; Zhao, Y.; Zhao, C. Transient simulation and thermodynamic analysis of pumped thermal electricity storage based on packed-bed latent heat/cold stores. *Renew. Energy* **2021**, *174*, 939–951. [CrossRef]
3. Gallo, A.B.; Simõões-Moreira, J.R.; Costa, H.K.M.; Santos, M.M.; Moutinho dos Santos, E.M. Energy storage in the energy transition context: A technology review. *Renew. Sustain. Energy Rev.* **2016**, *65*, 800–822. [CrossRef]
4. Petrollese, M.; Cascetta, M.; Tola, V.; Cocco, D.; Cau, G. Pumped thermal energy storage systems integrated with a concentrating solar power section: Conceptual design and performance evaluation. *Energy* **2022**, *247*, 123516. [CrossRef]
5. Mazzucco, G.; Xotta, G.; Salomoni, V.; Giannuzzi, M.; Maiorana, C. Solid thermal storage with PCM materials. Numerical investigations. *Appl. Therm. Eng.* **2017**, *124*, 545–559. [CrossRef]
6. Benato, A.; Stoppato, A. Pumped Thermal Electricity Storage: A technology overview. *Therm. Sci. Eng. Prog.* **2018**, *6*, 301–315. [CrossRef]
7. Rabi, A.M.; Radulovic, J.; Buick, J.M. Comprehensive Review of Compressed Air Energy Storage (CAES) Technologies. *Thermo* **2023**, *3*, 104–126. [CrossRef]
8. Rabi, A.M.; Radulovic, J.; Buick, J.M. Comprehensive Review of Liquid Air Energy Storage (LAES) Technologies. *Energies* **2023**, *16*, 6216. [CrossRef]
9. Alva, G.; Liu, L.; Huang, X.; Fang, G. Thermal energy storage materials and systems for solar energy applications. *Renew. Sustain. Energy Rev.* **2017**, *68*, 693–706. [CrossRef]
10. Alva, G.; Lin, Y.; Fang, G. An overview of thermal energy storage systems. *Energy* **2018**, *144*, 341–378. [CrossRef]
11. Chen, X.; Zhang, Z.; Qi, C.; Ling, X.; Peng, H. State of the art on the high-temperature thermochemical energy storage systems. *Energy Convers. Manag.* **2018**, *177*, 792–815. [CrossRef]
12. Rao, L.H.; Dirbude, S. Numerical modelling and optimization of packed-bed thermal-energy storage system. *J. Phys. Conf. Ser.* **2022**, *2178*, 012003. [CrossRef]
13. Pelay, U.; Luo, L.; Fan, Y.; Stitou, D.; Rood, M. Thermal energy storage systems for concentrated solar power plants. *Renew. Sustain. Energy Rev.* **2017**, *79*, 82–100. [CrossRef]
14. Kuravi, S.; Trahan, J.; Goswami, D.Y.; Rahman, M.M.; Stefanakos, E.K. Thermal energy storage technologies and systems for concentrating solar power plants. *Prog. Energy Combust. Sci.* **2013**, *39*, 285–319. [CrossRef]
15. Juul, G. *Numerical Modelling of a Packed Bed Thermal Energy Storage for Applications in a Carnot Battery*; KTH Royal Institute of Technology: Stockholm, Sweden, 2023.
16. Singh, H.; Saini, R.; Saini, J. A review on packed bed solar energy storage systems. *Renew. Sustain. Energy Rev.* **2010**, *14*, 1059–1069. [CrossRef]
17. Balakrishnan, A.R.; Pei, D.C.T. Heat Transfer in Gas-Solid Packed Bed Systems. The Conduction Mode. *Ind. Eng. Chem. Process. Des. Dev.* **1979**, *18*, 40–46. [CrossRef]
18. Almendros-Ibáñez, J.; Fernández-Torrijos, M.; Díaz-Heras, M.; Belmonte, J.; Sobrino, C. A review of solar thermal energy storage in beds of particles: Packed and fluidized beds. *Sol. Energy* **2019**, *192*, 193–237. [CrossRef]
19. Anzelius, A. Heating by means of percolating media. *J. Appl. Math. Mech.* **1926**, *6*, 291–294. [CrossRef]
20. Schumann, T. Heat transfer: A liquid flowing through a porous prism. *J. Frankl. Inst.* **1929**, *208*, 405–416. [CrossRef]
21. Torab, H.; Beasley, D.E. Optimization of a Packed Bed Thermal Energy Storage Unit. *J. Sol. Energy Eng.* **1987**, *109*, 170–175. [CrossRef]
22. McTigue, J.D.; Markides, C.N.; White, A.J. Performance response of packed-bed thermal storage to cycle duration perturbations. *J. Energy Storage* **2018**, *19*, 379–392. [CrossRef]
23. Bruch, A.; Molina, S.; Esence, T.; Fourmigué, J.; Couturier, R. Experimental investigation of cycling behaviour of pilot-scale thermal oil packed-bed thermal storage system. *Renew. Energy* **2017**, *103*, 277–285. [CrossRef]
24. Sanderson, T.; Cunningham, G. Performance and efficient design of packed bed thermal storage systems. *Part Appl. Energy* **1995**, *50*, 119–132. [CrossRef]
25. Regin, A.F.; Solanki, S.; Saini, J. An analysis of a packed bed latent heat thermal energy storage system using PCM capsules: Numerical investigation. *Renew. Energy* **2009**, *34*, 1765–1773. [CrossRef]
26. COMSOL Multiphysics. Porous Media Flow Module. 2020. Available online: https://doc.comsol.com/5.6/doc/com.comsol.help.porous/PorousMediaFlowModuleUsersGuide.pdf (accessed on 15 May 2024).
27. Bataineh, K.; Gharaibeh, A. Optimal design for sensible thermal energy storage tank using natural solid materials for a parabolic trough power plant. *Sol. Energy* **2018**, *171*, 519–525. [CrossRef]
28. de Gracia, A.; Cabeza, L.F. Numerical simulation of a PCM packed bed system: A review. *Renew. Sustain. Energy Rev.* **2017**, *69*, 1055–1063. [CrossRef]
29. Elouali, A.; Kousksou, T.; El Rhafiki, T.; Hamdaoui, S.; Mahdaoui, M.; Allouhi, A.; Zeraouli, Y. Physical models for packed bed: Sensible heat storage systems. *J. Energy Storage* **2019**, *23*, 69–78. [CrossRef]
30. Balakrishnan, A.R.; Pei, D.C.T. Heat Transfer in Gas-Solid Packed Bed Systems. A Critical Review. *Ind. Eng. Chem. Process. Des. Dev.* **1979**, *18*, 30–40. [CrossRef]

31. Zanganeh, G.; Pedretti, A.; Haselbacher, A.; Steinfeld, A. Design of packed bed thermal energy storage systems for high-temperature industrial process heat. *Appl. Energy* **2015**, *137*, 812–822. [CrossRef]
32. Meier, A.; Winkler, C.; Wuillemin, D. Experiment for modelling high temperature rock bed storage. *Sol. Energy Mater.* **1991**, *24*, 255–264. [CrossRef]
33. White, A.J.; McTigue, J.D.; Markides, C.N. Analysis and optimisation of packed-bed thermal reservoirs for electricity storage applications. *Proc. Inst. Mech. Eng. Part A J. Power Energy* **2016**, *230*, 739–754. [CrossRef]
34. Xu, C.; Wang, Z.; He, Y.; Li, X.; Bai, F. Sensitivity analysis of the numerical study on the thermal performance of a packed-bed molten salt thermocline thermal storage system. *Appl. Energy* **2012**, *92*, 65–75. [CrossRef]
35. De Lemos, M.J. *Turbulence in Porous Media: Modeling and Applications*, 2nd ed.; Elsevier: London, OH, USA, 2012; pp. 286–357. ISBN 978-08-098241-0.
36. Nandi, B.R.; Bandyopadhyay, S.; Banerjee, R. Numerical modeling and analysis of dual medium thermocline thermal energy storage. *J. Energy Storage* **2018**, *16*, 218–230. [CrossRef]
37. Kuravi, S.; Trahan, J.; Goswami, Y.; Jotshi, C.; Stefanakos, E.; Goel, N. Investigation of a High-Temperature Packed-Bed Sensible Heat Thermal Energy Storage System With Large-Sized Elements. *J. Sol. Energy Eng.* **2016**, *135*, 041008. [CrossRef]
38. Gil, A.; Medrano, M.; Martorell, I.; Lázaro, A.; Dolado, P.; Zalba, B.; Cabeza, L.F. State of the art on high temperature thermal energy storage for power generation. Part 1—Concepts, materials and modellization. *Renew. Sustain. Energy Rev.* **2010**, *14*, 31–55. [CrossRef]
39. Zhao, Y.; Zhao, C.; Wen, T.; Markides, C.N. High Temperature Sensible Storage—Industrial Applications. *Encycl. Energy Storage* **2022**, *1*, 424–432. [CrossRef]
40. Rahman, M.; Oni, A.O.; Gemechu, E.; Kumar, A. Assessment of energy storage technologies: A review. *Energy Convers. Manag.* **2020**, *223*, 113295. [CrossRef]
41. Villasmil, W.; Fischer, L.J.; Worlitschek, J. A review and evaluation of thermal insulation materials and methods for thermal energy storage systems. *Renew. Sustain. Energy Rev.* **2018**, *103*, 71–84. [CrossRef]